Title: Evapotranspiration of tropical peat swamp forests

Running title: Evapotranspiration of tropical PSFs

Takashi Hirano*, Kitso Kusin**, Suwido Limin* and Mitsuru Osaki*

*Research Faculty of Agriculture, Hokkaido University, Sapporo 060-8589, Japan

**CIMTROP, University of Palangkaraya, Palangkaraya 73112, Indonesia

Correspondence: Takashi Hirano, tel/fax +81-11-706-3689, e-mail:
hirano@env.agr.hokudai.ac.jp

Keywords: disturbances, drainage, eddy covariance, energy balance, ENSO, fire, groundwater level, smoke, Southeast Asia

Abstract

In Southeast Asia, peatland is widely distributed and has accumulated a massive amount of soil carbon, coexisting with peat swamp forest (PSF). The peatland, however, has been rapidly degraded by deforestation, fires and drainage for the last two decades. Such disturbances change hydrological conditions, typically groundwater level (*GWL*), and accelerate oxidative peat decomposition. Evapotranspiration (*ET*) is a major determinant of *GWL*, whereas information on the *ET* of PSF is limited. Therefore, we measured *ET* using the eddy covariance technique for four to six years between 2002 and 2009, including El Niño and La Niña events, at three sites in Central Kalimantan, Indonesia. The sites were different in disturbance degree: a PSF with little drainage (UF), a heavily drained PSF (DF) and a drained burnt ex-PSF (DB); *GWL* was significantly lowered at DF, especially in the dry season. The *ET* showed a clear seasonal variation with a peak in the mid-dry season and a large decrease in the late dry season, mainly following seasonal variation in net radiation (R_n). The R_n drastically decreased with dense smoke from peat fires in the late dry season. Annual *ET* forced to close energy balance for four years was 1636 ± 53, 1553 ± 117 and 1374 ± 75 mm yr^{-1} (mean ± 1 standard deviation), respectively, at UF, DF and DB. The undrained PSF (UF) had high and rather stable annual *ET*, independently of El Niño and La Niña events, in comparison with other tropical rainforests. The minimum monthly-mean *GWL* explained 80% of interannual variation in *ET* for the forest sites (UF and DF); the positive relationship between *ET* and *GWL* indicates that drainage by a canal decreased *ET* at DF through lowering *GWL*. In addition, *ET* was decreased by 16% at DB in comparison with UF chiefly because of vegetation loss through fires.

Introduction

In Southeast Asia, mainly Indonesia and Malaysia, peatland is widely distributed, coexisting with swamp forest, over an area of 2.48×10^5 km^2 and accumulating up to 68.5 Pg of soil organic carbon, which accounts for 11-14% of global peat carbon (Page *et al.*, 2011). These peatlands, however, have been rapidly devastated by deforestation and drainage for logging and land-use change, with such disturbances often causing frequent large-scale peat fires (Miettinen *et al.*, 2012b; Page *et al.*, 2002). As a result, the proportion of forest cover in the peatlands of Peninsular Malaysia, Sumatra and Borneo fell from 77% to 36% from 1990 to 2010 (Miettinen *et al.*, 2012b). In these regions, 20% of peatlands had been also converted to plantations of oil palm and Acacia by 2010 (Miettinen *et al.*, 2012a). These human pressures have increased the vulnerability of the huge peat carbon pool and increased the risk for the pool to be a large carbon source to the atmosphere chiefly because of peat fires and lowered groundwater level (*GWL*) which stimulates the rate of biological oxidation (e.g. Hirano *et al.*, 2012; Page *et al.*, 2002).

The carbon balance of peatland is chiefly controlled by local hydrology (e.g. Bozkurt *et al.*, 2001; Limpens *et al.*, 2008), which determines the water regime of surface peat. Under unsaturation conditions, peat is aerated, and its soil organic compounds are easily oxidized into carbon dioxide (CO_2). Therefore, theoretically, drainage to lower *GWL* enhances oxidative peat decomposition and its resultant CO_2 emissions. Field studies have illustrated such relationship with *GWL* from studies of peat subsidence (Couwenberg *et al.*, 2009; Hooijer *et al.*, 2010; Hooijer *et al.*, 2012) and soil CO_2 efflux (Hirano *et al.*, 2014; Jauhiainen *et al.*, 2012; Sundari *et al.*, 2012) in tropical peatlands. Also, Hirano *et al.* (2012) showed that the CO_2 balance of tropical peat ecosystems was clearly related to *GWL* on both monthly and annual bases.

The *GWL* results from water balance. Because tropical peatland is typically

ombrotrophic (Dommain *et al.*, 2011; Page *et al.*, 2004), *GWL* varies according to residuals (storage change) between precipitation as input and evapotranspiration (*ET*) and discharge as output. Although precipitation can be also affected by large-scale deforestation (Spracklen *et al.*, 2012), *ET* and runoff are directly affected by deforestation, fires and drainage, respectively (e.g. Bosch & Hewlett, 1982; Dore *et al.*, 2010; Sun *et al.*, 2001). For example, conversion from tropical forest to pasture decreased *ET* in Amazonia, especially in the dry season (von Randow *et al.*, 2004). To predict *GWL* under human pressures and thereby assess the carbon balance of tropical peatland, it is crucial to quantify *ET* and elucidate the effects of disturbances on *ET*. In addition, tropical forest plays an important role in hydrologic and atmospheric circulations, which drive climate systems, both on regional and global scales by massive *ET* and its resultant strong evaporative cooling (Bonan, 2008). Although peat swamp forest in Malaysia and Indonesia except Papua (7.00×10^4 km^2, Miettinen *et al.*, 2012b) accounts for only 5% of the forest area in the two countries (1.29×10^6 km^2, Harris *et al.*, 2012) in 2000, it is important to investigate the energy balance of tropical peat swamp forest for better understanding of the ecosystem function of tropical forest, because its ground water condition is different from that of other upland forest. Information on the energy balance and *ET* of tropical peatland is still quite limited (Hirano *et al.*, 2005).

We measured fluxes of sensible heat (*H*) and latent heat (*lE*) using the eddy covariance technique and determined *ET* and energy balance at three sites within 15 km of each other on tropical peatland near Palangkaraya, Central Kalimantan, Indonesia (Hirano *et al.*, 2012). The sites were different in disturbance degree: a peat swamp forest (PSF) with little drainage (UF), a heavily drained PSF (DF) and a drained burnt ex-PSF with limited vegetation (DB). Here we show the results of field measurement for four to six years between 2002 and 2009, including El Niño and La Niña events and discuss seasonal and interannual variations in the *ET* of PSF and the effects of anthropogenic disturbances due to drainage and fires on the *ET*.

Materials and Methods

Study site

The study was conducted in tropical peatlands near Palangkaraya, Central Kalimantan province, Indonesia. A large peatland area was deforested and drained in this province during the late 1990s according to a national project: the Mega Rice Project. Although the project was terminated in 1999, it left vast degraded peatland. Three sites were located on flat terrain within 15 km (Hirano *et al.*, 2012): a PSF with little drainage (UF; 2.32°S, 113.90°E), a drained PSF (DF; 2.35°S, 114.14°E) and a drained burnt ex-PSF with re-growing vegetation (DB; 2.34°S, 114.04°E), which was dominated by fern plants. The DF and DB have been drained by a large canal (25 m wide × 3.5-4.5 m deep) excavated in 1996 and 1997. Information of each site was detailed by our previous paper (Hirano *et al.*, 2012).

Flux measurement

Eddy fluxes of sensible heat (H) and latent heat (lE) were measured on towers since July 2004 at a height of 36.5 m, November 2001 at 41.3 m and April 2004 at 3.0 m, respectively, at UF, DF and DB using the eddy covariance technique with a sonic anemometer-thermometer (CSAT3; Campbell Scientific Inc., USA) and an open-path CO_2/H_2O analyzer (LI7500; Li-Cor Inc., USA) (Hirano *et al.*, 2012). Sensor signals were recorded using a datalogger (8421; Hioki E. E. Corp., Japan) at 10 Hz. Net radiation (R_n) and albedo were measured with a radiometer (CNR-1; Kipp & Zonen, the Netherlands) at a height of 36.3, 40.6 and 3.3 m, respectively, at UF, DF and DB. Air temperature and relative humidity were measured with a platinum resistance thermometer and a capacitive hygrometer (HMP45; Vaisala, Finland) installed in a non-ventilated radiation shield (DTR503A; Vaisala) at a height of 36.3, 41.7 and 1.5 m, respectively, at UF, DF and DB. Precipitation was measured with a tipping-bucket rain gauge (TE525; Campbell Scientific Inc.) at a height of 41.0 m at DF. Sensor signals were

112 measured every 30 s; their half-hourly means were recorded using a datalogger (CR10X;
113 Campbell Scientific Inc.). Groundwater level (*GWL*), which was shown as a distance between
114 the ground (reference) and groundwater surfaces, was measured every 30 min with a water
115 level logger (DL/N; Sensor Technik Sirnach AG, Sienach, Switzerland or DCX-22 VG; Keller
116 AG, Winterthur, Switzerland) within 5 m from towers at the three sites.
117
118 *Flux calculation*
119 Half-hourly mean *H* and *lE* were calculated according to the following procedures: 1) removal
120 of noise spikes (Vickers & Mahrt, 1997), 2) planar fit rotation (Wilczak *et al.*, 2001), 3) water
121 vapor correction for *H* (Hignett, 1992), 4) correction for high- and low-frequency losses using
122 a theoretical transfer function (Massman, 2000, Massman, 2001), 5) covariance calculation
123 using a block average and 6) density fluctuation correction for *lE* (Webb *et al.*, 1980).
124 The sensitivity of an open-path analyzer (LI7500) for water vapor density was
125 calibrated by comparing half-hourly mean water vapor densities from the LI7500 and a
126 slow-response thermometer/hygrometer (HMP45) (Iwata *et al.*, 2012), because the sensitivity
127 directly affects the covariance of water vapor density and vertical wind velocity. The
128 sensitivity was calculated every day as the slope of correlation between two water vapor
129 densities (*y*: LI7500, *x*: HMP45) using a moving window of 31 days, and then the daily
130 variation of the slope was smoothed by fitting a tenth-order spline curve. If correlation was
131 not significant ($p > 0.05$), the slope data were excluded from the fitting. Before the correlation
132 analysis, data were excluded in the rain and in the nighttime to avoid outliers due to raindrops
133 or dew condensation on the LI7500's window. In addition to such data screening, data were
134 only used under the neutral condition of atmospheric stability for DB, because the LI7500
135 was installed 1.5 m higher than the HMP45. The reciprocal of the daily slope was applied as a
136 correction coefficient for the covariance.

We used flux data from July 2004 to August 2008, December 2001 to July 2008 and April 2004 to September 2009, respectively, for UF, DF and DB. To calculate annual sums, we defined the annual period of 365 or 366 days starting on July 10 or 11 (DOY192) and ending on July 9 or 10 (DOY191) (Hirano *et al.*, 2012). The whole rainy season was captured in each annual period, because the rainy season usually starts in October and lasts until June in this area (Hirano *et al.*, 2012). In the period, annual sums were calculated for the four year periods of 2004–2008, the six year periods of 2002–2008 and the five year periods of 2004–2009, respectively, for UF, DF and DB.

Quality control and gap filling of flux data

We first excluded flux data obtained during rain and when the mean wind direction was within ±30°, ±35° and ±20° from the north, respectively, for UF, DF and DB, thereby avoiding flow distortion caused by the tower. The azimuth angles were determined from tower dimensions. Next, we calculated the difference between covariances determined from the whole interval of 30 min and six intervals of 5 min. Flux data were excluded, if covariance difference was larger than 250% (Foken & Wichura, 1996). Consequently, the survival rates of H and lE data available for annual summations were 49% and 51%, 50% and 50%, and 46% and 64%, respectively, for UF, DF and DB. Data gaps were filled by the look-up table (LUT) method using R_n and vapor pressure deficit (VPD) as predictors on a half-hourly basis. The R_n and VPD were grouped into ten and three classes, respectively. The LUT was created every three months: November–January, February–April, May–July and August–October, considering climate conditions (Hirano *et al.*, 2007). After gap filling, to correct annual ET for the energy imbalance (Table S1), H and lE were forced to balance with R_n (adjustment) using a ratio of H and lE (Bowen ratio) on a daily basis (Twine *et al.*, 2000).

Calculation of bulk parameters

Bulk parameters of surface conductance (G_s) (Monteith, 1965), decoupling factor (Ω) (Jarvis & McNaughton, 1986) and Priestley-Taylor coefficient (α) (Priestley & Taylor, 1972) were calculated to interpret the seasonal variation and environmental response of *ET*. To avoid instability and divergence, the bulk parameters around midday from 1000 to 1400 in no-rain conditions were only used to calculate monthly means for the analysis (Ryu *et al.*, 2008). Also, albedo for shortwave radiation was calculated for the midday period when global radiation was larger than 700 W m^{-2} (Hirano *et al.*, 2007).

The G_s (m s^{-1}) stands for the integration of individual leaf's stomatal conductance for transpiration and surface wetness for evaporation, which was calculated backward from the Penman-Monteith equation by replacing $R_n - G$ with $H + lE$, because G was unavailable (Eqn. 1). This substitution would overestimate G_s because of energy imbalance (Table S1).

$$\frac{1}{G_s} = \frac{1}{G_a}\left[\frac{\varepsilon(H+lE)+\rho C_p G_a \frac{VPD}{\gamma}}{lE} - \varepsilon - 1\right] \quad (1)$$

where G_a is bulk aerodynamic conductance (m s^{-1}), ε is s/γ, s is the slope of relationship between saturation vapor pressure and temperature (kPa K^{-1}), γ is psychrometric constant (= 0.067 kPa K^{-1}), ρ is air density (kg m^{-3}), C_p is specific heat of air at constant pressure (= 1007 J kg^{-1} K^{-1}), *VPD* is vapor pressure deficit (kPa). The G_a was calculated using the following equation (Humphreys *et al.*, 2006).

$$G_a = \left[\frac{2}{\kappa u^*}\left(\frac{dh}{dv}\right)^{\frac{2}{3}} + \frac{u}{u^{*2}}\right]^{-1} \quad (2)$$

where κ is von Karman constant (=0.4), u^* is friction velocity (m s^{-1}), *dh* is thermal diffusivity, *dv* is molecular diffusivity of water vapor and *u* is mean wind velocity (m s^{-1}). The ratio of *dh* and *dv* (*dh*/*dv*) was set at 0.89 (Humphreys *et al.*, 2006).

The Ω is an index (0 to 1) of decoupling between vegetation and the atmosphere for *ET*, which was defined as follows:

$$\Omega = \frac{\varepsilon+1}{\varepsilon+1+\frac{G_a}{G_s}} \quad (3)$$

The Ω approaches 0 when *ET* is controlled by G_s and *VPD* (coupling), and approaches one when *ET* is controlled by available energy (decoupling).

The α is the ratio of measured *lE* and equilibrium *lE* (lE_{eq}), which is the *lE* of an extended wet surface (Priestley & Taylor, 1972). The α was calculated using the following equation (Flint & Childs, 1991).

$$\alpha = \frac{lE}{lE_{eq}} = \frac{lE}{\frac{(Rn-G)s}{s+\gamma}} \cong \frac{lE}{\frac{(H+lE)s}{s+\gamma}} = \frac{s+\gamma}{(1+\beta)s} \quad (4)$$

where β is Bowen ratio.

Results

Seasonal variation

Monthly values of environmental elements, energy fluxes and bulk parameters are shown in time sequence in Fig. 1. Precipitation shows seasonality with fluctuations due to El Niño and La Niña events. According to sea surface temperature (SST) anomaly in the Niño 3.4 region, El Niño and La Niña events occurred in the 02-03, 04-05 and 06-07 periods and the 05-06, 07-08 and 08-09 periods, respectively (NOAA, http://www.cpc.ncep.noaa.gov/products/analysis_monitoring/ensostuff/ensoyears.stml). Following the precipitation variation, *GWL* and *VPD* varied seasonally. In 2004 and 2005, the less-vegetated ground surface at DB was studded with open water, which lowered albedo. A large increase in albedo in 2006, especially at DB, was due to strong surface desiccation caused by El Niño drought (Hirano *et al.*, 2007). A massive amount of smoke emitted from large-scale peat fires, which often occurs during El Niño drought, led to sudden reduction in R_n in 2002 and 2006 (Hirano *et al.*, 2007; Hirano *et al.*, 2012; Hirano *et al.*, 2005).

To clarify seasonal variation, monthly values were ensemble averaged for each site for the common period of four years from August 2004 through July 2008 (Fig. 2). In addition, monthly values were averaged for the rainy and dry seasons, respectively (Table 1); the threshold to separate the two seasons was monthly precipitation of 100 mm (e.g. Malhi *et al.*, 2002). As a result, 10 months out of a total (48 months) were classified as the dry season. On average for the four years, August and September were in the dry season, and July with monthly precipitation of 102 mm was the transition between the two seasons (Fig. 2). The *GWL* reached its minimum of -0.55, -1.05 and -0.52 m at UF, DF and DB, respectively, in October and was significantly lower in the dry season than in the rainy season. Midday *VPD* began to increase in April and peaked in September at UF (1.84 kPa) and DF (1.92 kPa) and in October at DB (2.28 kPa); it was significantly higher in the dry season. Albedo showed

seasonality similar to that of *VPD* with a peak in October at UF and DF and in November at DB, which differed significantly between the two seasons except for DB. The R_n showed an opposite peak in October because of shading due to dense smoke in 2006 (Fig. 1). However, seasonal difference in R_n was not significant, because R_n is usually larger in the dry season if no fires occur. Smoke from peat fires is critical for the radiation environment in the dry season (Hirano *et al.*, 2012). The *H* increased significantly in the dry season at DB, whereas its seasonality was obscure at UF and DF. The *lE* or *ET* increased gradually from April through August and decreased during September and October; the decrease would correspond to R_n decrease. Seasonal difference in *lE* was significant only at UF. Similarly with *H*, Bowen ratio increased significantly in the dry season only at DB. The ratio of *lE* and R_n increased significantly in the dry season at UF and DF, except for DB. The G_s began to decrease in July and reached an opposite peak in October at UF and DF and in November at DB, which resembles *GWL* or the mirror image of midday *VPD* in seasonal variation, whereas significant seasonal difference was detected only at DF, at which seasonal variation in *GWL* was the largest. The Ω continued to decrease from July through October and showed significant differences between the two seasons at the all sites. Although α showed a decreasing tendency from July through October at DB, no significant seasonal variation was detected at all the sites.

Interannual variation

Annual values of environmental elements, energy fluxes and bulk parameters are listed in Table 2. Annual precipitation was 2446 ± 50 mm yr^{-1} (mean ± 1 SD) on average for four annual periods from the 04-05 through 07-08 periods; its interannual variation was small with a coefficient of variance (CV) of 2.1%. Thus, the PSF is categorized into “tropical rainforest” or “humid tropical forest” by the definition of annual precipitation > 1500 mm yr^{-1} and dry

season length < 6 months (Lewis, 2006). Annual dry period length (DPL), which is defined as the number of days with 30-day moving total of precipitation less than 100 mm (Kume *et al.*, 2011), averaged out at 90 ± 33 days yr^{-1} with a CV of 34.2% for the same period. For the seven years from the 02-03 period, annual precipitation was 2445 ± 90 mm yr^{-1} (CV: 3.8%). On the other hand, seven-year mean annual precipitation was calculated at 2411 ± 393 mm yr^{-1} (CV: 16.3%), if precipitation was summed following the solar calendar from 1 January 2002. Although the two means of annual precipitation were very similar each other independently of summation periods, their SD values differed by a factor of 4.4. The annual period starting on DOY 191, which can include almost the whole of one continuous rainy season (Fig. 2), had much smaller interannual variation in precipitation than the solar calendar period, because total precipitation in the rainy season was independent of its duration in Indonesia (Hamada *et al.*, 2002). This comparison reveals that annual precipitation depends on its summation period.

The annual precipitation was rather stable, whereas DPL increased in the 02-03 and 6-07 periods because of the prolonged dry season due to El Niño drought. Following the interannaul variation in the precipitation pattern, *GWL*, midday *VPD* and R_n showed significant interannual difference (Table 3), whereas R_n was strongly affected by smoke from peat fires. Also, there was significant interannual difference both in adjusted and unadjusted *ET* to close energy balance, although their CVs were relatively small (<7.5%). Adjusted *ET* was the highest in the 07-08 period (La Niña) and the lowest in the 06-07 period (El Niño), which corresponds to the order of annual R_n. Among bulk parameters, only Ω differed significantly.

Environmental response of ET

The relationship of *ET* with environmental elements was analysed using daily values of *lE* and *H* under the condition that the gap ratio of half-hourly *lE* or *H* was lower than 20% for the daytime from 600 through 1800 (Fig. 3). Both *lE* and *H* showed a significant linear relationship, respectively, with R_n at the all sites. At DB, however, *lE* and *H* were apart from the lines downward and upward, respectively, in the dry season in 2004 (Fig. 1), when vegetation was still sparse and surface soil was desiccated. The lE / R_n averaged out at 0.84, 0.75 and 0.68, respectively, at UF, DF and DB. The *lE* showed a significant quadratic relationship with *GWL*, which is a principal hydrological variable with a large annual amplitude. The r^2 value was the largest at DF with the largest *GWL* range. The *lE* normalized by R_n (lE / R_n) showed a weak negative liner relationship with *GWL* at the all sites. On the other hand, there was no relationship between lE / R_n and midday *VPD* (data not shown), which is related to evaporative demand.

Adjusted annual *ET* showed a significant positive linearity ($p < 0.01$) with the minimum monthly-mean *GWL* at each site with r^2 vales of 0.98, 0.85 and 0.97, respectively, at UF, DF and DB (data not shown). The r^2 values were much larger than against annual mean *GWL*. The strong linearity suggests that the minimum monthly-mean *GWL* drawdown by 10 cm decreases annual *ET* by 19, 33 and 26 mm, respectively, at UF, DF and DB. Moreover, as a whole, adjusted annual *ET* at the two forest sites showed a significant combined correlation ($r^2 = 0.80$, $p < 0.01$) (Fig. 4). Therefore, we can say that the minimum monthly-mean *GWL* is a robust total predictor of annual *ET* of PSF, because the minimum *GWL* determines not only the water regime in the dry season but also peat fire occurrence (Takahashi & Limin, 2011), which drastically affects the radiation environment (Fig. 1).

For a further analysis, bulk parameters of G_s were plotted against *GWL* (Fig. 5). Data were classified into three groups according to *VPD*, and quadratic curves were fitted to all data groups, because many tree species decrease stomatal conductance in flooding (e.g.

294 Kozlowski, 1997). Significant convex curves ($p < 0.05$), except for a high *VPD* group at DB,
295 show that G_s didn't decrease simply as *GWL* decreased. At UF, the curves suggest that G_s
296 peaked at *GWL*s of -0.10, -0.14 and -0.13 m, respectively, for *VPD* of <1.4, 1.4-1.9 and >1.9
297 kPa. Although G_s was lower at higher *VPD*, it was almost identical independently of *VPD* in
298 flooding conditions at DB, suggesting weak stomatal control on G_s. It was reported that some
299 flooding-tolerant trees acclimated to flooding and stomatal conductance recovered within a
300 flooding period (Herrera, 2013). At UF, however, there was no significant difference in G_s
301 (16.8 ± 6.2 vs. 16.5 ± 6.9 mm s^{-1} (mean $\pm$ 1 SD)) under the flooding condition (*GWL* > 0.0 m)
302 between the early (until February) and late (after March) rainy seasons. To compare the
303 response of G_s to *GWL* variation, data of the three sites were plotted together under the high
304 *VPD* condition (> 1.9 kPa) (Fig. 5d). The G_s began to decrease when *GWL* lowered below a
305 threshold at each site. The *GWL* threshold for G_s decrease was the lowest at DF, followed by
306 UF and DB in order.
307
308 *Inter-site comparison*
309 Seasonal means and annual values were compared among the three sites (Tables 1 to 3). The
310 *GWL*, which was measured as a distance between the ground and groundwater surfaces, was
311 significantly lower at DF because of drainage, whereas *GWL* at DB was very close to that of
312 UF in spite of the fact that DB was drained at the same time as DF. The relatively high *GWL*
313 at DB was chiefly caused by large ground subsidence due to peat fires (Hirano *et al.*, 2014).
314 The R_n was significantly smaller at DB only in the rainy season probably because of
315 scattering open water surfaces. Midday *VPD* was significantly higher at DB chiefly owing to
316 lower *lE* and higher air temperature (data not shown). Albedo was significantly lower at DB
317 than UF only in the rainy season. The *H* was significantly larger at DB both in the rainy and
318 dry seasons.

Mean annual *ET* before adjustment to the energy balance for the four annual periods was 1529 ± 65, 1365 ± 68 and 1197 ± 52 mm yr^{-1} (mean ± 1 SD), respectively, for UF, DF and DB. Uncertainties shown as one SD in annual *ET* due to random errors, which were assessed according to our previous study (Hirano et al., 2012), were estimated to be 16 ± 3, 17 ± 2 and 10 ± 1 mm yr^{-1}, respectively, for UF, DF and DB. The annual *ET* was the largest at UF, followed by DF and DB in order, whereas *lE* showed no significant difference between DF and DB in the dry season. After the adjustment, annual *ET* increased to 1636 ± 53, 1553 ± 117 and 1374 ± 75 mm yr^{-1}, respectively, for UF, DF and DB; *ET* was significantly smaller at DB than at UF and DF. As a result, Bowen ratio was the highest at DB both in the rainy and dry seasons; it was significantly higher at DF than UF only in the rainy season. The G_s was the highest at UF, followed by DF and DB in order, whereas no significant difference was found between DF and DB in the dry season. The Ω was significantly higher at UF only in the rainy season. The α was significantly lower at DB.

Discussion

Comparison of annual ET between PSF and other tropical forests

Unadjusted and adjusted annual *ET*s of an almost undrained PSF (UF) were 1529 ± 65 and 1636 ± 53 mm yr^{-1}, respectively, which accounted for 63% and 67% of annual precipitation (*P*: 2446 ± 50 mm yr^{-1}), respectively. The CV was 3.2% and 2.0%, respectively, for adjusted *ET* and precipitation. Although the interannual variation of *ET* shown as CV was larger than that of precipitation, it was smaller than those of tropical rainforests in Malaysian Borneo (5.6%, Kume *et al.*, 2011) and Peninsular Malaysia (4.0%, Kosugi *et al.*, 2011). The annual *ET* of UF was more than those of upland tropical rainforests in Malaysian Borneo (estimated *ET* using a big-leaf model: 1323 ± 74 mm yr^{-1}, P: 2600 ± 272 mm yr^{-1}, *ET* / *P*: 0.51; Kume *et al.*, 2011), Peninsular Malaysia (adjusted *ET*: 1287 ± 52 mm yr^{-1}, *P*: 1865 ± 288 mm yr^{-1}, *ET* / *P*: 0.69; Kosugi *et al.*, 2011), central Amazonia (unadjusted *ET*: 1123 mm yr^{-1}, *P*: 2089 mm yr^{-1}, *ET* / *P*: 0.54; Malhi *et al.*, 2002), central Amazonia (unadjusted *ET*: 1123 ± 9 mm yr^{-1}, *P*: 2091 ± 215 mm yr^{-1}, *ET* / *P*: 0.54; Hutyra *et al.*, 2007) and southwest China (adjusted *ET*: 1029 ± 29 mm yr^{-1}, *P*: 1322 ± 78 mm yr^{-1}, *ET* / *P*: 0.78; Li *et al.*, 2010), a floodplain forest in Amazonia (adjusted *ET*: 1332 ± 21 mm yr^{-1}, *P*: 1692 ± 181 mm yr^{-1}, *ET* / *P*: 0.79; Borma *et al.*, 2009), a wet montane cloud forest in Hawaii (adjusted *ET*: 1232 mm yr^{-1}, *P*: 2401 mm yr^{-1}, *ET* / *P*: 0.51; Giambelluca *et al.*, 2009) and the average of tropical forests in Asia and Oceania regions (20°S-20°N) (*ET*: 1255 ± 329 mm yr^{-1}, *P*: 2577 ± 1057 mm yr^{-1}, *ET* / *P*: 0.49 (*n* = 57); Komatsu *et al.*, 2012), whereas it was less than that of a wet tropical forest in Costa Rica (estimated *ET* using the Priestley-Taylor model: 2139 ± 176 mm yr^{-1}, *P*: 3732 ± 281 mm yr^{-1}, *ET* / *P*: 0.57; Loescher *et al.*, 2005). Although the evaporative fraction to precipitation (*ET* / *P*) was lower in UF than in tropical rainforests in Peninsular Malaysia (0.69) and southwest China (0.78) and an Amazonian floodplain forest (0.79), the PSF with high *GWL* is ranked high among moist tropical forests with annual precipitation more than 2000 mm yr^{-1} (Kume *et*

358 *al.*, 2011). In comparison with a tropical rainforest in Malaysian Borneo (Kume *et al.*, 2011),
359 the PSF at UF had 13% more R_n and 52% higher *VPD* (0.76 kPa) on an annual basis. This
360 higher evaporative demand is a potential reason of the higher *ET* of the PSF, together with
361 high *GWL*.
362
363 *Environmental response of ET*
364 The *ET* was chiefly controlled by R_n at all the sites, because the relationship between *ET* and
365 *GWL* or *VPD* was weak. The R_n determined the temporal variation of *lE* by 54, 65 and 59%
366 (r^2), respectively, at UF, DF and DB on a daily basis (Fig. 3). Evaporative fractions (lE / R_n)
367 were on average 0.84, 0.75 and 0.68, respectively, at UF, DF and DB. Fisher *et al.* (2009)
368 showed a positive relationship between *lE* and R_n with high r^2 of 0.87 and an evaporative
369 fraction of 0.72 from a synthesis analysis of 21 pan-tropical eddy covariance sites. We can say
370 that the PSF at UF with a higher evaporative fraction has a high evaporative ability among
371 tropical ecosystems. As a result, the PSF showed a low Bowen ratio of 0.19 in comparison
372 with an average (0.30) of the 21 tropical sites (Fisher *et al.*, 2009).
373 The *lE* showed relatively clear seasonal variation (Fig. 2); *lE* continued to increase from
374 the late rainy season to the mid-dry season and decreased in the late-dry season. The annual
375 amplitudes of the seasonal variation in *lE* were 2.6, 2.2 and 2.7 MJ m^{-2} day^{-1} on a monthly
376 basis, respectively, at UF, DF and DB, which were equivalent to *ET*s of 1.07, 0.92 and 1.10
377 mm day^{-1}, respectively. A similar *ET* increase in the dry season was also reported for tropical
378 forests in Amazonia (da Rocha *et al.*, 2004; Hasler & Avissar, 2007; Hutyra *et al.*, 2007) and
379 Thailand (Tanaka *et al.*, 2008), which was attributed to increased R_n and the lack of drought
380 stress due to deep root systems. The *lE* decrease in the late dry season was enhanced during El
381 Niño drought in 2002 and 2006, when peat fires occurred and consequently R_n decreased
382 sharply (Fig. 1). However, lE / R_n increased conversely even during the peat fires, except for

383 at DB in 2004. These facts indicate that the *lE* decrease in the late dry season was chiefly
384 caused by R_n decrease due to smoke or haze and evaporative efficiency on R_n didn't decrease
385 even in such drought conditions. As a result, *lE* / R_n remained high during the late rainy
386 season and the dry season (Fig. 2). On the other hand, G_s continued to decrease during the dry
387 season probably because of stomatal closure due to water stress by *GWL* decrease and *VPD*
388 increase (Fig. 5). The decreases from July to October or November were 5.3, 6.5 and 4.3 mm
389 s^{-1}, respectively, at UF, DF and DB. Thus, relatively stable *lE* / R_n during the dry season was
390 probably attributed to the compensation of G_s decrease and *VPD* increase. Severe drought in
391 2006 decreased G_s remarkably (Fig. 1). Correspondingly, Ω largely decreased during the dry
392 season, especially at DB with sparse, low vegetation. Although many tree species decrease
393 stomatal conductance in flooding (e.g. Kozlowski, 1997), the effect of flooding on G_s was
394 limited (Fig. 5) and was not reflected on the seasonal variation of G_s (Fig. 2), because
395 enhanced evaporation from the flooded ground would compensate the decrease of
396 transpiration due to stomatal closure.
397
398 *Effects of drainage and fires*
399 The *ET* measurement started at DF about five years after the excavation of a large canal,
400 which has functioned as effective drainage. Thus, *GWL* was significantly lower at DF than at
401 UF (Table 3). The difference in *GWL* between the two forest sites was larger in the dry season
402 than in the rainy season; *GWL* difference was on average 0.37 m in February-April and 0.50
403 m in October (Fig. 2). As a result, the annual range of *GWL* was larger at DF (0.79 m) than at
404 UF (0.66 m). Especially in El Niño years, the *GWL* difference increased in the late dry season
405 (Fig. 1). The lowering of the minimum *GWL* decreased annual *ET* linearly (Fig. 4). However,
406 no significant difference in adjusted annual *ET* was found between DF and UF by paired *t*-test
407 (p = 0.085), although mean annual *ET* was 5% less at DF (Table 2).

Although G_s was significantly lower at DF than UF both in the rainy and dry seasons (Table 1), a *GWL* threshold, at which G_s began to decrease, was much lower at DF than at UF (Fig. 5d), suggesting the adaptation of tree species at DF to the low *GWL* environment during more than five years after canal excavation. There is a report that 83% of root biomass of a PSF in the same area as UF was distributed in the surface soil layer of 0-0.25 m in depth and remaining 17% was in the underlying layer of 0.25-0.50 m (Sulistiyanto, 2004). Roots of PSF trees are concentrated in the surface peat level in comparison with deeply-rooted upland tropical forests (e.g. Davidson *et al.*, 2011; Nesptad *et al.*, 1994). Tree roots probably penetrated deeper into seasonally unsaturated soil following *GWL* lowering. Annual evaporative fraction (lE / R_n) increased linearly (r^2 = 0.88) for six years from the 02-03 to 07-08 periods at DF. In addition, G_s at DF was averaged in a drought condition (*GWL*: -1.4 to -1.2 m, *VPD*: 2.0 to 2.5 kPa) for each of three El Niño events in 2002, 2004 and 2006; the means were 6.3 ± 2.5, 8.5 ± 3.9 and 7.8 ± 2.8 mm s^{-1}, respectively, for 2002, 2004 and 2006. As a result, mean G_s in 2002 was significantly lower than those in 2004 and 2006 (Tukey's HSD, $p < 0.05$). These facts support the hypothesis of adaptation. The G_s and *ET* most probably decreased by *GWL* lowering due to drainage at DF, because G_s was significantly lower in the dry season only at DF (Table 1) and annual *ET* showed a positive correlation with the minimum *GWL* (Fig. 4). However, the drainage effect would be eased gradually because of the adaptation through root redistribution.

The DB, a burnt site with regrowing vegetation, was drained together with DF by a canal running between the two sites, whereas *GWL* at DB was very close to that at UF, because the ground subsided largely owing to peat fires (Hirano *et al.*, 2014). Adjusted annual *ET* of 1374 ± 75 mm yr^{-1}, which accounted for 56% of annual precipitation, was significantly lower than those of the other two forest sites because of low tree density; the annual *ET* was equivalent to 84% and 88% of UF and DF, respectively (Tables 2 and 3). However, the annual *ET* was

compatible with that of a tropical rainforest in Malaysian Borneo (Kume *et al.*, 2011). Conversely, annual *H* was significantly higher than those at UF and DF, and consequently Bowen ratio was significantly higher. Generally, albedo is higher in unforested areas with short vegetation than in forest (e.g. Bonan, 2008), which can result in lower R_n in unforested areas. In Amazonia, land conversion from forest to pasture increased albedo by 55% and decreased R_n by 13% (von Randow *et al.*, 2004). Midday albedo at a pasture and an upland rice field in Amazonia were reported to be 0.15-0.17 (Sakai *et al.*, 2004). At DB, however, annual mean midday albedo was 0.087 ± 0.007 and showed no significant difference with the forest sites. Also, annual R_n showed no significant difference, whereas it was smaller by 6% than that at UF. The unexpected lower albedo at DB was attributable to dark color of burnt peat and scattered open water. On the other hand, annual mean G_s was less than 50% of that at UF (Table 2) chiefly owing to low leaf area index. Although G_s showed no significant difference between the rainy and dry seasons (Table 1), inter-site difference between DB and UF increased by 50% in the dry season. The G_s responded to *GWL* lowering more sensitively than those of UF and DF (Fig. 5); G_s began to decrease at about -0.1 m. This sensitive response could be due to the shallow rooting depth (von Randow *et al.*, 2012) of the regrowing vegetation, which was dominated by fern and sedge plants (Hirano et al., 2012). Tree loss due to fires and subsequent vegetation succession decreased G_s and consequently *ET*, whereas the decrease in *ET* was less than expected by G_s decrease, because albedo didn't decrease, midday *VPD* increased and *GWL* remained high owing to large subsidence (Fig. 2).

Annual discharge can be calculated from precipitation and *ET* to be 810 ± 53, 893 ± 105 and 1072 ± 71 mm yr^{-1}, respectively, at UF, DF and DB, on the assumption that storage change is negligible on an annual basis. Although no significant difference was found between UF and DF, annual discharge tended to increase by drainage and significantly increased by tree loss due to fires. A negative linear relationship was found between inter-site

458 difference in annual discharge (DF minus UF) and the minimum monthly *GWL* at DF ($p <$
459 0.05) (data not shown). The increase of discharge potentially increases fluvial organic carbon
460 outflow (Moore *et al.*, 2013). Our results indicate that disturbances due to drainage and fires
461 decreased *ET* and increased discharge; the effect of drainage was remarkable in El Niño years
462 with lower *GWL*. This study can contribute to a better assessment of the water balance of PSF
463 by providing reliable information on *ET* to hydrological models and improve our knowledge
464 of the carbon dynamics of PSF through a better prediction of *GWL* which is determined as a
465 result of water balance.
466

Acknowledgements

This work was supported by JSPS Core University Program, JSPS KAKENHI (Nos. 13375011, 15255001, 18403001, 21255001 and 25257401) and the JST-JICA Project (SATREPS) (Wild Fire and Carbon Management in Peat-Forest in Indonesia).

References

Bonan G (2008) Forests and climate change: forcings, feedbacks, and the climate benefits of forests. *Science,* **320**, 1444-1449.

Borma LS, da Rocha H. R., Cabral OM *et al*. (2009) Atmosphere and hydrological controls of the evapotranspiration over a floodplain forest in the Bananal Island region, Amazonia. *Journal of Geophysical Research*, **114**, G01003, doi:10.1029/2007JG000641.

Bosch J, Hewlett J (1982) A review of catchment experiments to determine the effect of vegetation changes on water yield and evapotranspiration. *Journal of Hydrology,* **55**, 3-23.

Bozkurt S, Lucisano M, Moreno L, Neretnieks I (2001) Peat as a potential analogue for the long-term evolution in landfills. *Earth-Science Reviews,* **53**, 95-147.

Couwenberg J, Dommain R, Joosten H (2009) Greenhouse gas fluxes from tropical peatlands in south-east Asia. *Global Change Biology,* **16**, 1715-1732.

da Rocha HR, Goulden ML, Miller SD, Menton MC, Pinto LDVO, de Freitas HC, Figueira AMES (2004) Seasonality of waer and heat fluxes over a tropical forest in eastern Amazonia. *Ecological Applications*, **14**, S22-S32.

Davidson E, Lefebvre PA, Brando PM *et al.* (2011) Carbon inputs and water uptake in deep soils of an eastern Amazon forest. *Forest Science,* **57**, 51-58.

Dommain R, Couwenberg J, Joosten H (2011) Development and carbon sequestration of tropical peat domes in south-east Asia: links to post-glacial sea-level changes and Holocene climate variability. *Quaternary Science Reviews,* **30**, 999-1010.

Dore S, Kolb TE, Montes-Helu M *et al.* (2010) Carbon and water fluxes from ponderosa pine forests disturbed by wildfire and thinning. *Ecological Applications,* **20**, 663-683.

Fisher JB, Malhi Y, Bonal D *et al.* (2009) The land-atmosphere water flux in the tropics. *Global Change Biology,* **15**, 2694-2714.

497 Flint AL, Childs SW (1991) Use of the Priestley-Taylor evaporation equation for soil water
498 limited conditions in a small forest clearcut. *Agricultural and Forest Meteorology,* **56**,
499 247-260.
500 Foken T, Wichura B (1996) Tools for quality assessment of surface-based flux measurements.
501 *Agricultural and Forest Meteorology,* **78**, 83-105.
502 Giambelluca T, Martin R, Asner G *et al.* (2009) Evapotranspiration and energy balance of
503 native wet montane cloud forest in Hawai‘i. *Agricultural and Forest Meteorology,* **149**,
504 230-243.
505 Hamada J, Yamanaka MD, Matsumoto J, Fukao S, Winarso PA, Sribimawati T (2002) Spatial
506 and temporal variations of the rainy season over Indonesia and their link to ENSO.
507 *Journal of the Meteorological Society of Japan,* **80**, 285-310.
508 Harris NL, Brown S, Hagen SC *et al.* (2012) Baseline map of carbon emissions from
509 deforestation in tropical regions. *Science,* **336**, 1573-1576.
510 Hasler N, Avissar R (2007) What controls evapotranspiration in the Amazon basin? *Journal of*
511 *Hydrometeorology,* **8**, 380-395.
512 Herrera A (2013) Responses to flooding of plant water relations and leaf gas exchange in
513 tropical tolerant trees of a black-water wetland. *Frontiers in Plant Science,* **4**,
514 doi:10.3389/fpls.2013.00106.
515 Hignett P (1992) Corrections to temperature measurements with a sonic anemometer.
516 *Boundary-Layer Meteorology,* **61**, 175-187.
517 Hirano T, Kusin K, Limin S, Osaki M (2014) Carbon dioxide emissions through oxidative
518 peat decomposition on a burnt tropical peatland. *Global Chang Biology,* **20**, 555-565.
519 Hirano T, Segah H, Harada T, Limin S, June T, Hirata R, Osaki M (2007) Carbon dioxide
520 balance of a tropical peat swamp forest in Kalimantan, Indonesia. *Global Change*
521 *Biology,* **13**, 412-425.

522 Hirano T, Segah H, Kusin K, Limin S, Takahashi H, Osaki M (2012) Effects of disturbances
523 on the carbon balance of tropical peat swamp forests. *Global Change Biology,* **18**,
524 3410-3422.
525 Hirano T, Segah H, Limin S *et al.* (2005) Energy balance of a tropical peat swamp forest in
526 Central Kalimantan, Indonesia. *Phyton-Annales Rei Botanicae,* **45**, 67-71.
527 Hooijer A, Page S, Canadell JG, Silvius M, Kwadijk J, Wosten H., Jauhiainen J. (2010)
528 Current and future CO_2 emissions from drained peatlands in Southeast Asia.
529 *Biogeosciences,* **7**, 1505-1514.
530 Hooijer A, Page S, Jauhiainen J, Lee WA, Lu XX, Idris A, Anshari G (2012) Subsidence and
531 carbon loss in drained tropical peatlands. *Biogeosciences,* **9**, 1053-1071.
532 Humphreys ER, Lafleur PM, Flanagan LB, Hedstrom N, Syed KH, Glenn AJ, Granger R
533 (2006) Summer carbon dioxide and water vapor fluxes across a range of northern
534 peatlands. *Journal of Geophysical Research,* **111**, G04011,
535 doi:10.1029/2005JG000111.
536 Hutyra LR, Munger JW, Saleska SR *et al.* (2007) Seasonal controls on the exchange of carbon
537 and water in an Amazonian rain forest. *Journal of Geophysical Research,* **112**, G03008,
538 doi:10.1029/2006JG000365.
539 Iwata H, Harazono Y, Ueyama M (2012) Sensitivity and offset changes of a fast-response
540 open-path infrared gas analyzer duting long-term observations in an Arctic
541 environment. *Journal of Agricultural Meteorology,* **68**, 175-181.
542 Jarvis PG, Mcnaughton KG (1986) Stomatal control of transpiration: scaling up from leaf to
543 region. *Advances in Ecological Research,* **15**, 1-49.
544 Jauhiainen J, Hooijer A, Page SE (2012) Carbon dioxide emissions from an *Acacia* plantation
545 on peatland in Sumatra, Indonesia. *Biogeosciences*, **9**, 617-630.
546 Komatsu H, Cho J, Matsumoto K, Otsuki K (2012) Simple modeling of the global variation in

annual forest evapotranspiration. *Journal of Hydrology,* **420-421**, 380-390.

Kosugi Y, Takanashi S, Tani M *et al.* (2012) Effect of inter-annual climate variability on evapotranspiration and canopy CO_2 exchange of a tropical rainforest in Peninsular Malaysia. *Journal of Forest Research,* **17**, 227-240.

Kozlowski KK (1997) Responses of woody plants to flooding and salinity. *Tree Physiology Monograph,* **1**, 1-29.

Kume T, Tanaka N, Kuraji K *et al.* (2011) Ten-year evapotranspiration estimates in a Bornean tropical rainforest. *Agricultural and Forest Meteorology,* **151**, 1183-1192.

Lewis SL (2006) Tropical forests and the changing earth system. *Philosophical Transactions of The Royal Society, Biological Sciences,* **361**, 195-210.

Li Z, Zhang Y, Wang S, Yuan G, Yang Y, Cao M (2010) Evapotranspiration of a tropical rain forest in Xishuangbanna, southwest China. *Hydrological Processes,* **24**, 2405-2416.

Limpens J, Berendse F, Blodau C *et al.* (2008) Peatlands and the carbon cycle: from local processes to global implications - a synthesis. *Biogeosciences,* **5**, 1475-1491.

Loescher HW, Gholz HL, Jacobs JM, Oberbauer SF (2005) Energy dynamics and modeled evapotranspiration from a wet tropical forest in Costa Rica. *Journal of Hydrology,* **315**, 274-294.

Malhi Y, Pegoraro E, Nobre AD, Pereira MGP, Grace J, Culf AD, Clement R (2002) The energy and water dynamics of a central Amazonian rain forest. *Journal of Geophysical Research,* **107**, 8061, doi:10.1029/2001JD000623

Massman WJ (2000) A simple method for estimating frequency response corrections for eddy covariance systems. *Agricultural and Forest Meteorology,* **104**, 185-198.

Massman WJ (2001) Reply to comment by Rannik on "A simple method for estimating frequency response for eddy systems". *Agricultural and Forest Meteorology,* **107**, 247-251.

572 Miettinen J, Hooijer A, Shi C et al. (2012a) Extent of industrial plantations on Southeast
573 Asian peatlands in 2010 with analysis of historical expansion and future projections.
574 *GCB Bioenergy,* **4**, 908-918.
575 Miettinen J, Shi C, Liew SC (2012b) Two decades of destruction in Southeast Asia's peat
576 swamp forests. *Frontiers in Ecology and the Environment,* **10**, 124-128.
577 Monteith JL (1965) Evaporation and the environment. *Symposium of the Sciety of Exploratory*
578 *Biology,* **19**, 205-234.
579 Moore S, Evans CD, Page SE et al. (2013) Deep instability of deforested tropical peatlands
580 revealed by fluvial organic carbon fluxes. *Nature*, **493**, 660-664.
581 Nesptad DC, de Carvalho CR, Davidson EA et al. (1994) The role of deep roots in the
582 hydrological and carbon cycles of Amazonian forests and pastures. *Nature,* **372**,
583 666-669.
584 Page SE, Rieley JO, Banks CJ (2011) Global and regional importance of the tropical peatland
585 carbon pool. *Global Change Biology,* **17**, 798-818.
586 Page SE, Siegert F, Rieley JO, Boehm HDV, Jaya A, Limin S (2002) The amount of carbon
587 released from peat and forest fires in Indonesia during 1997. *Nature,* **420**, 61-65.
588 Page SE, Wűst RaJ, Weiss D, Rieley JO, Shotyk W, Limin SH (2004) A record of Late
589 Pleistocene and Holocene carbon accumulation and climate change from an equatorial
590 peat bog (Kalimantan, Indonesia): implications for past, present and future carbon
591 dynamics. *Journal of Quaternary Science,* **19**, 625-635.
592 Priestley CHB, Taylor RJ (1972) On the assessment of surface heat flux and evaporation
593 using large-scale parameters. *Monthly Weather Review,* **100**, 81-92.
594 Ryu Y, Baldocchi DD, Ma S, Hehn T (2008) Interannual variability of evapotranspiration and
595 energy exchange over an annual grassland in California. *Journal of Geophysical*
596 *Research*, **113**, D09104, doi:10.1029/2007JD009263.

Sakai RK, Fitzjarrald DR, Moraes OLL *et al.* (2004) Land-use change effects on local energy, water, and carbon balances in an Amazonian agricultural field. *Global Change Biology,* **10**, 895-907.

Spracklen DV, Arnold SR, Taylor CM (2012) Observations of increased tropical rainfall preceded by air passage over forests. *Nature*, **489**, 282-285.

Sulistiyanto Y (2004) Nutrient dynamics in different sub-types of peat sawmp forest in Central Kalimantan, Indonesia. Ph. D. thesis, The University of Nottingham, 387 pp.

Sun G, Mcnulty S, Shepard J *et al.* (2001) Effects of timber management on the hydrology of wetland forests in the sourthern United States. *Forest Ecology and Management,* **143**, 227.

Sundari S, Hirano T, Yamada H, Kusin K, Limin S (2012) Effects of groundwater level on soil respiration in tropical peat swamp forests. *Journal of Agricultural Meteorology,* **68**, 121-134.

Takahashi H, Limin SH (2011) Water in peat and peat fire in tropical peatland. In: *Third International Workshop on: Wild Fire and Carbon Management in Peat-forest in Indonesia.* (eds Osaki M, Takahashi H, Honma T *et al.*) pp. 49-54, Hokkaido University and University of Palangkaraya.

Tanaka N, Kume T, Yoshifuji N *et al.*, (2008) A review of evapotranspiration estimates from tropical forests in Thailand and adjacent regions. *Agricultural and Forest Meteorology,* **148**, 807-819.

Twine TE, Kustas WP, Norman JM *et al.* (2000) Correcting eddy-covariance flux underestimates over a grassland. *Agricultural and Forest Meteorology,* **103**, 279-300.

Vickers D, Mahrt L (1997) Quality control and flux sampling probelms for tower and aircraft data. *Journal of Atmospheric and Oceanic Technology,* **14**, 512-526.

von Randow C, Manzi AO, Kruijt B *et al.* (2004) Comparative measurements and seasonal

variations in energy and carbon exchange over forest and pasture in South West Amazonia. *Theoretical and Applied Climatology*, **78**, 5-26.

von Randow RCS, von Randow C, Hutjes RWA, Tomasella J, Kruijt B (2012) Evapotranspiration of deforested areas in central and southwestern Amazonia. *Theoretical and Applied Climatology*, **109**, 205-220.

Webb EK, Pearman GI, Leuning R (1980) Correction of flux measurements for density effects due to heat and water vapor transfer. *Quarterly Journal of the Royal Meteorological Society*, **106**, 85-106.

Wilczak JM, Oncley SP, Stage SA (2001) Sonic anemometer tilt correction algorithms. *Boundary-Layer Meteorology*, **106**, 85-106.

Supporting Information

Additional Supporting Information is available in the online version of this article:

Data S1. Supporting text describing energy imbalance, including references and summary table (Table S1).

Table 1 Comparison of environmental elements, energy fluxes and surface parameters between the rainy and dry seasons (mean ± 1 standard deviation).

Site	*GWL* (m)		Midday *VPD* (kPa)[1)]		R_n (MJ m^{-2} day^{-1})		Albedo		*H* (MJ m^{-2} day^{-1})		*lE* (MJ m^{-2} day^{-1})	
	Rainy	Dry	Rainy	Dry	Rainy	Dry	Rainy	Dry	Rainy	Dry	Rainy	Dry
UF	-0.06±0.25a	-0.43±0.26**, a	1.41±0.18a	1.77±0.14**	13.1±0.8a	12.9±2.2	0.090±0.003a	0.097±0.008**	1.94±0.30a	2.08±0.40a	9.94±0.81a	11.2±1.73**, a
DF	-0.45±0.30b	-0.94±0.35**, b	1.43±0.20a	1.84±0.14**	13.0±0.8a	12.4±2.5	0.086±0.005ab	0.096±0.010**	2.12±0.38a	2.46±0.80a	9.08±0.68b	9.20±1.58b
DB	-0.05±0.20a	-0.42±0.29**, a	1.71±0.31b	1.97±0.31*	12.4±0.7b	11.9±2.3	0.083±0.015b	0.094±0.015	2.55±0.39b	3.29±0.95**,b	7.95±0.73c	8.14±1.82b
p[2)]	<0.01	<0.01	<0.01	0.11	<0.01	0.63	0.04	0.84	<0.01	<0.01	<0.01	<0.01

Site	*ET* (mm day^{-1})		Bowen ratio		*lE* / R_n		G_s (mm s^{-1})		Ω		α	
	Rainy	Dry	Rainy	Dry	Rainy	Dry	Rainy	Dry	Rainy	Dry	Rainy	Dry
UF	4.09±0.33a	4.60±0.71**, a	0.20±0.03a	0.19±0.03a	0.76±0.07a	0.88±0.12**, a	15.6±2.9a	14.2±4.0a	0.60±0.06a	0.53±0.07**	1.01±0.04a	1.01±0.05a
DF	3.73±0.28b	3.78±0.65b	0.24±0.05b	0.27±0.08a	0.70±0.04b	0.75±0.06**, b	13.2±2.7b	10.4±3.5**, b	0.54±0.07b	0.47±0.08*	0.99±0.05a	0.96±0.07a
DB	3.27±0.30c	3.35±0.75b	0.32±0.06c	0.42±0.18**, b	0.64±0.06c	0.69±0.11b	7.4±1.7c	7.6±2.3b	0.56±0.11ab	0.48±0.15*	0.88±0.08b	0.86±0.09b
p	<0.01	<0.01	<0.01	<0.01	<0.01	<0.01	<0.01	<0.01	<0.01	0.49	<0.01	<0.01

1) Mean for midday from 1000 to 1400.
2) The *p*-value of ANOVA among the sites in each column.
3) Different alphabet letters in each column denote significant difference among the sites at a significance level of 0.05 according to Tukey's HSD.
4) The symbol of * or ** denote significant difference between the rainy and dry seasons at a significant level of 0.05 or 0.01, respectively, according to Student's *t*-test.

Table 2 Annual values of environmental elements, energy fluxes and bulk parameters

		02-03	03-04	04-05	05-06	06-07	07-08	08-09	Mean[1)]	1 SD	CV (%)[2)]
	Global radiation (GJ m^{-2} yr^{-1})	6.22	6.29	6.29	6.24	6.01	6.44	6.20	6.24	0.18	2.8
	Precipitation (mm yr^{-1})	2287	2459	2506	2456	2384	2438	2582	2446	50	2.1
	DPL (days)[3)]	146	105	105	53	123	78	139	90	31	34.2
	Mean *GWL* (m)			-0.15	-0.07	-0.25	-0.08		-0.14	0.08	61.2
	Minimum *GWL* (m)[4)]			-0.67	-0.51	-0.98	-0.33		-0.62	0.27	43.8
	R_n (GJ m^{-2} yr^{-1})			4.78	4.77	4.58	4.92		4.76	0.14	2.9
	Midday *VPD* (kPa)			1.46	1.41	1.59	1.50		1.49	0.07	5.0
	H (GJ m^{-2} yr^{-1})			0.70	0.72	0.73	0.73		0.72	0.02	2.1
	lE (GJ m^{-2} yr^{-1})			3.51	3.84	3.69	3.86		3.73	0.16	4.3
UF	Boweb ratio			0.20	0.19	0.20	0.19		0.19	0.01	3.4
	Unajusted *ET* (mm yr^{-1})			1442	1577	1515	1582		1529	65	4.3
	Adjusted *ET* (mm yr^{-1})[5)]			1634	1648	1566	1695		1636	53	3.3
	G_s (mm s^{-1})			14.2	17.6	15.1	16.1		15.7	1.4	9.2
	Ω			0.61	0.62	0.55	0.57		0.59	0.04	6.0
	α			1.00	1.03	1.00	1.03		1.01	0.02	1.7
	albedo			0.094	0.090	0.092	0.091		0.091	0.002	2.0
	Mean *GWL* (m)	-0.56	-0.56	-0.65	-0.47	-0.67	-0.40		-0.55	0.13	24.1
	Minimum *GWL* (m)[4)]	-1.27	-1.15	-1.37	-1.06	-1.56	-0.74		-1.18	0.36	30.5
	R_n (GJ m^{-2} yr^{-1})	4.59	4.76	4.71	4.79	4.41	4.87		4.70	0.20	4.3
	Midday *VPD* (kPa)	1.68	1.52	1.49	1.48	1.66	1.44		1.52	0.10	6.3
	H (GJ m^{-2} yr^{-1})	0.88	0.72	0.84	0.74	0.93	0.69		0.80	0.11	13.2
	lE (GJ m^{-2} yr^{-1})	3.16	3.32	3.22	3.38	3.18	3.54		3.33	0.17	5.0
DF	Boweb ratio	0.28	0.22	0.26	0.22	0.29	0.20		0.24	0.04	17.8
	Unajusted *ET* (mm yr^{-1})	1299	1364	1320	1386	1304	1453		1365	68	5.0
	Adjusted *ET* (mm yr^{-1})[5)]	1471	1601	1529	1611	1401	1671		1553	117	7.5
	G_s (mm s^{-1})	9.9	12.5	11.8	13.3	9.7	14.2		12.3	1.9	15.8
	Ω	0.51	0.57	0.55	0.57	0.49	0.47		0.52	0.05	9.2
	α	0.96	0.99	0.95	1.00	0.95	1.02		0.98	0.04	3.6
	albedo	0.089	0.088	0.087	0.083	0.091	0.090		0.088	0.003	3.9
	Mean *GWL* (m)			-0.20	-0.06	-0.23	-0.02	-0.02	-0.13	0.10	79.5
	Minimum *GWL* (m)[4)]			-0.72	-0.44	-0.92	-0.28	-0.34	-0.59	0.29	48.6
	R_n (GJ m^{-2} yr^{-1})			4.53	4.46	4.25	4.68	4.57	4.48	0.18	4.0
	Midday *VPD* (kPa)			1.74	1.65	1.86	1.82	1.62	1.77	0.09	5.4
	H (GJ m^{-2} yr^{-1})			1.05	0.93	1.03	0.94	0.89	0.99	0.06	6.2
	lE (GJ m^{-2} yr^{-1})			2.80	3.09	2.84	2.94	2.91	2.92	0.13	4.4
DB	Boweb ratio			0.38	0.30	0.36	0.32	0.31	0.34	0.03	10.2
	Unajusted *ET* (mm yr^{-1})			1150	1267	1165	1206	1194	1197	52	4.4
	Adjusted *ET* (mm yr^{-1})[5)]			1359	1404	1277	1454	1436	1374	75	5.5
	G_s (mm s^{-1})			7.07	8.01	6.68	7.67	7.52	7.36	0.60	8.1
	Ω			0.64	0.58	0.43	0.47	0.56	0.53	0.10	18.2
	α			0.87	0.91	0.86	0.87	0.88	0.88	0.02	2.3
	albedo			0.078	0.088	0.096	0.088	0.087	0.087	0.007	8.3

1) Mean for four annual periods from 04-05 through 07-08.
2) Coefficient of variance.
3) Dry period length, which is defined as days having a 30-day moving precipitation total of < 100 mm (Kume *et al.*, 2011).
4) The minimum monthly-mean *GWL*.
5) *ET* forced to close energy balance using Bowen ratio on a daily basis.

Table 3 The *p*-values from two-way ANOVA for sites and years without replication based on the data in Table 3.

		Site[1)]	Year
GWL	UF	a	0.001
	DF	b	
	DB	a	
R_n	UF		0.000
	DF	0.001	
	DB		
Midday*VPD*	UF	a	0.016
	DF	a	
	DB	b	
H	UF	a	0.151
	DF	a	
	DB	b	
lE or unadjusted *ET*	UF	a	0.014
	DF	b	
	DB	c	
Bowen ratio	UF	a	0.057
	DF	a	
	DB	b	
Adjusted *ET*	UF	a	0.002
	DF	a	
	DB	b	
G_s	UF	a	0.054
	DF	b	
	DB	c	
Ω	UF		0.023
	DF	0.100	
	DB		
α	UF	a	0.068
	DF	a	
	DB	b	
albedo	UF		0.365
	DF	0.424	
	DB		

1) Different alphabet letters in each column denote significant difference among the sites at a significance level of 0.05 according to Tukey's HSD.

Fig. 1. Time series of monthly values of environmental elements, energy fluxes and bulk parameters at the three sites (UF, DF and DB) between 2001 and 2009. The 3-month running mean of sea surface temperature anomalies in the Niño 3.4 region is shown (a). El Niño and La Niña events are characterized by a five consecutive 3-month means with thresholds above +0.5 and below -0.5°C, respectively (NOAA, http://www.cpc.ncep.noaa.gov/products/analysis_monitoring/ensostuff/ensoyears.stml). *GWL*: groundwater level, midday *VPD*: vapor pressure deficit between 1000 and 1400, R_n: net radiation, *H*: sensible heat flux, *lE*: latent heat flux, G_s: bulk surface conductance, Ω: decoupling coefficient, α: Priestley-Taylor coefficient.

Fig. 2. Mean seasonal variations in monthly values of environmental elements, energy fluxes and bulk parameters at the three sites (UF, DF and DB) from August 2004 to July 2008. *GWL*: groundwater level, midday *VPD*: vapor pressure deficit between 1000 and 1400, R_n: net radiation, *H*: sensible heat flux, *lE*: latent heat flux, G_s: bulk surface conductance, Ω: decoupling coefficient, α: Priestley-Taylor coefficient.

Fig. 3. Relationships between energy fluxes and environmental elements at the three sites (UF, DF and DB) on a daily basis. Lines (a, b, c, g, h and i) and quadratic curves (d, e and f) were fitted ($p < 0.05$). Grey symbols at DB (c) were measurements in the dry season in 2004, which were excluded from the fitting. *H*: sensible heat flux, *lE*: latent heat flux, R_n: net radiation, *GWL*: groundwater level.

Fig. 4. Combined relationship between annual evapotranspiration (*ET*) and the minimum monthly- mean groundwater level (*GWL*) for UF and DF. A significant line was fitted ($p < 0.01$).

Fig. 5. Relationships between bulk surface conductance (G_s) and groundwater level (*GWL*) at UF (a), DF (b) and DB (c). Data were divided into three groups according to vapor pressure deficit (*VPD*) and a quadratic curve was fitted to each group ($p < 0.05$). Data in each *VPD* group were binned into deciles by *GWL*. The relationships are compared among the three sites using the deciles in a high VPD condition (> 1.9 kPa) (d). Dark grey symbols at DB (c) were measurements in the dry season in 2004, which were excluded from the fitting.

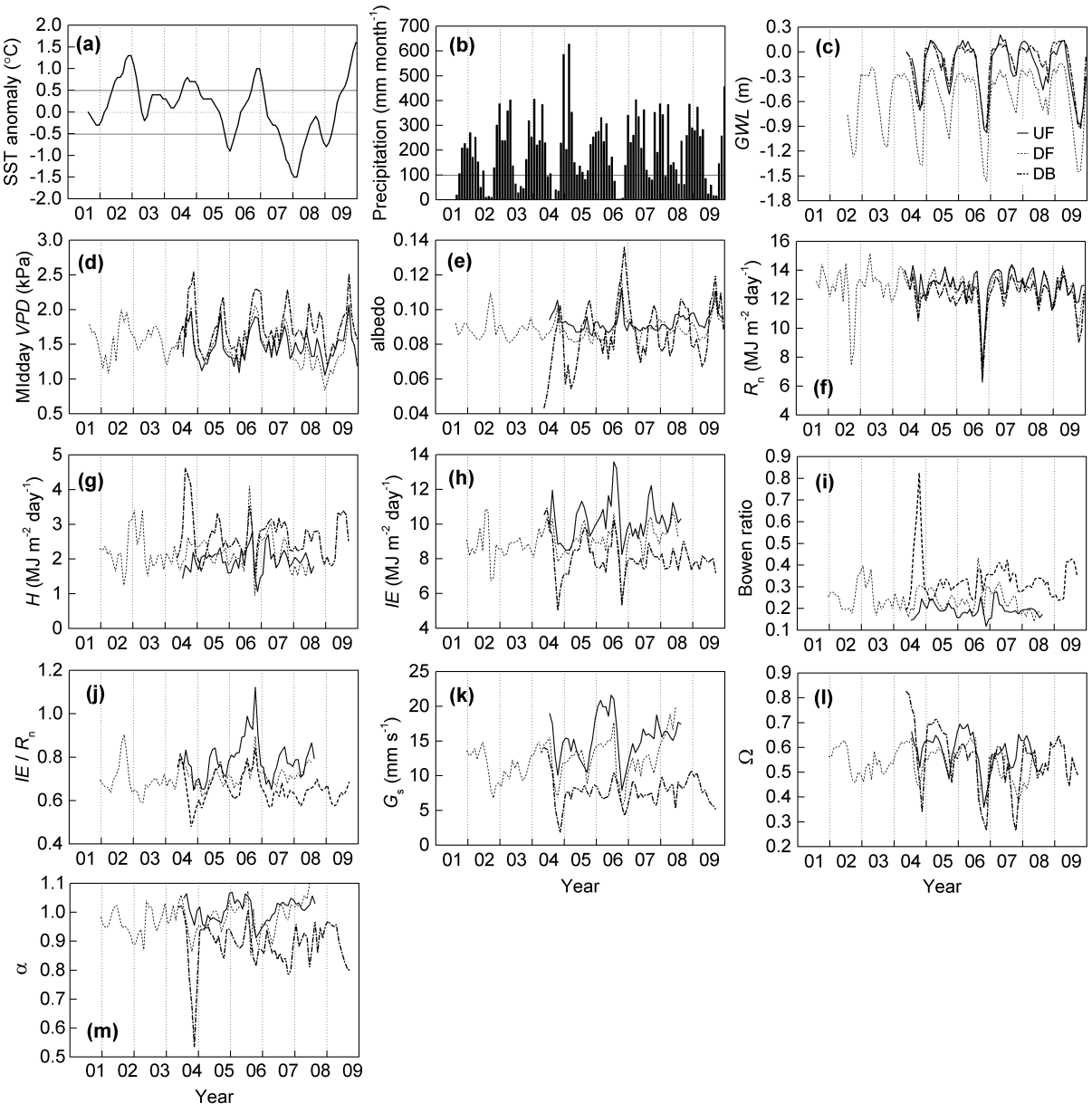
(a)
SST anomaly (°C)
(b)
Precipitation (mm month-1)
(c)
GWL (m)
UF
DF
DB
(d)
Midday VPD (kPa)
(e)
albedo
(f)
Rn (MJ m-2 day-1)
(g)
H (MJ m-2 day-1)
(h)
IE (MJ m-2 day-1)
(i)
Bowen ratio
(j)
IE / Rn
(k)
Gs (mm s-1)
(l)
Ω
(m)
α
Year
Year

Fig. 1

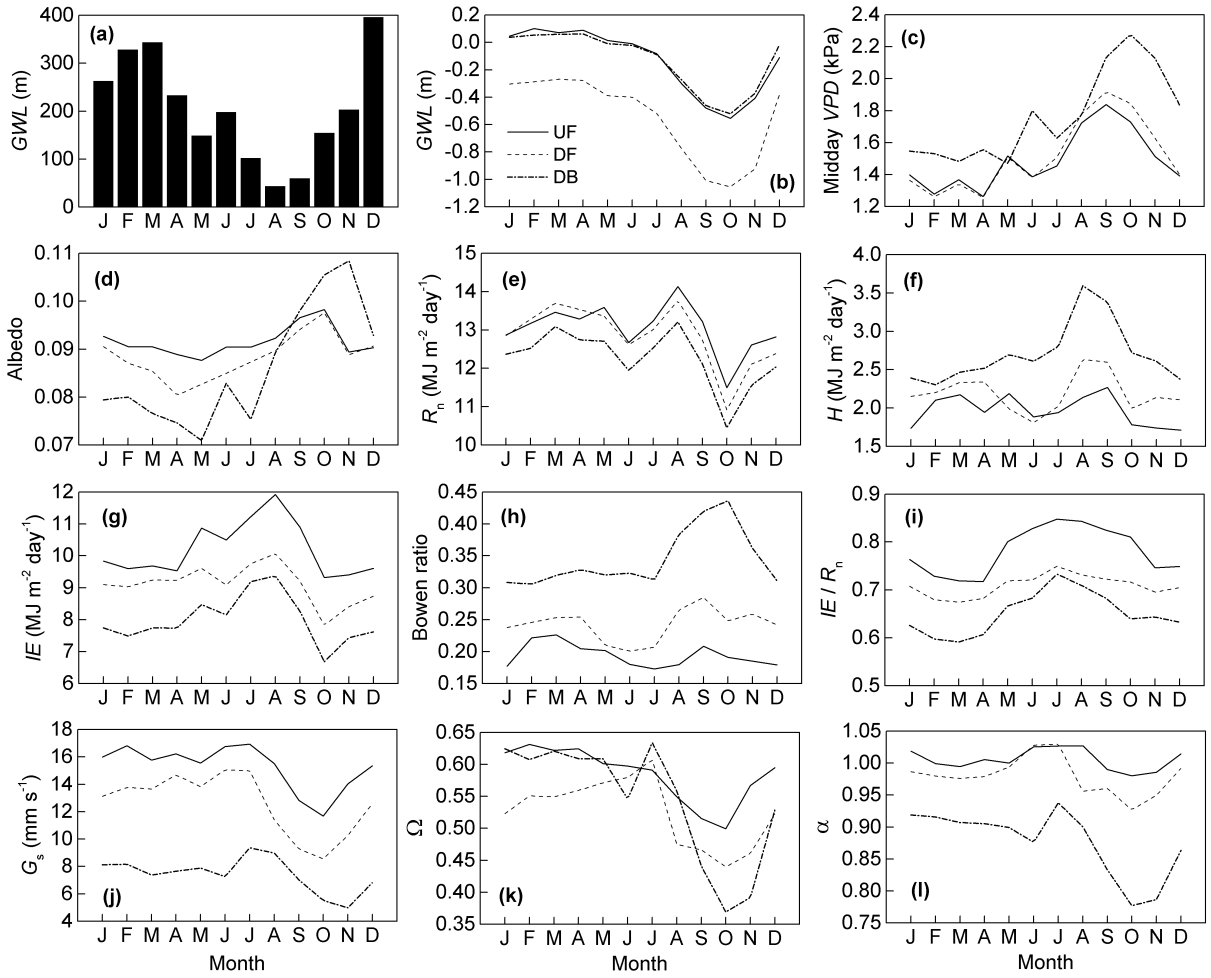
(a)
GWL (m)
(b)
UF
DF
DB
(c)
Midday VPD (kPa)
(d)
Albedo
(e)
Rn (MJ m-2 day-1)
(f)
H (MJ m-2 day-1)
(g)
IE (MJ m-2 day-1)
(h)
Bowen ratio
(i)
IE / Rn
(j)
Gs (mm s-1)
(k)
Ω
(l)
α
J F M A M J J A S O N D
Month

Fig. 2

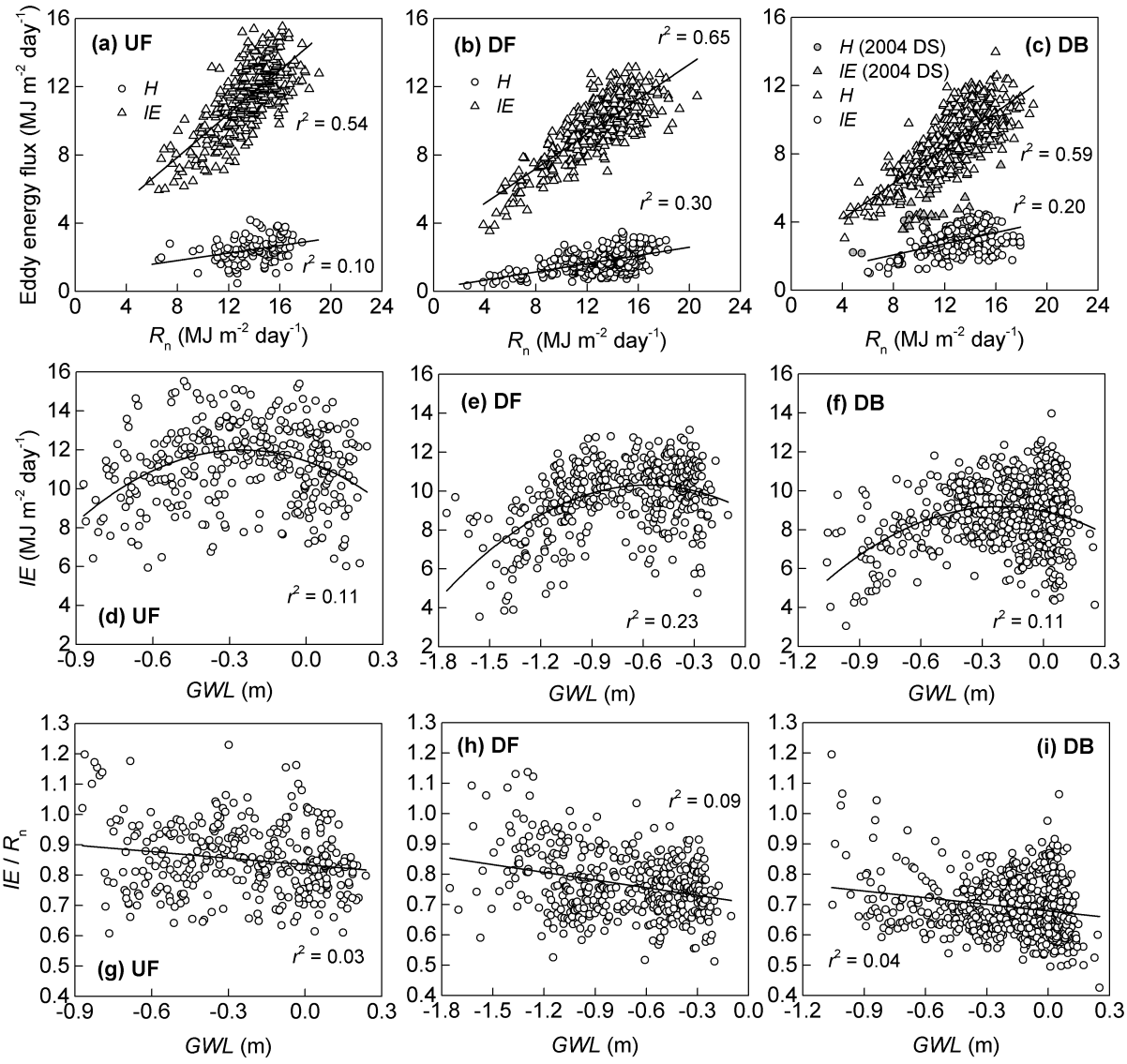
(a) UF
H
IE
r² = 0.54
r² = 0.10
Eddy energy flux (MJ m⁻² day⁻¹)
Rn (MJ m⁻² day⁻¹)
(b) DF
r² = 0.65
r² = 0.30
(c) DB
H (2004 DS)
IE (2004 DS)
r² = 0.59
r² = 0.20
(d) UF
r² = 0.11
IE (MJ m⁻² day⁻¹)
GWL (m)
(e) DF
r² = 0.23
(f) DB
r² = 0.11
(g) UF
r² = 0.03
IE / Rn
(h) DF
r² = 0.09
(i) DB
r² = 0.04

Fig. 3

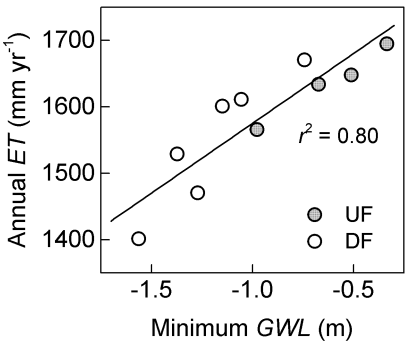
Annual ET (mm yr-1)
1700
1600
1500
1400
r2 = 0.80
UF
DF
-1.5
-1.0
-0.5
Minimum GWL (m)

Fig. 4

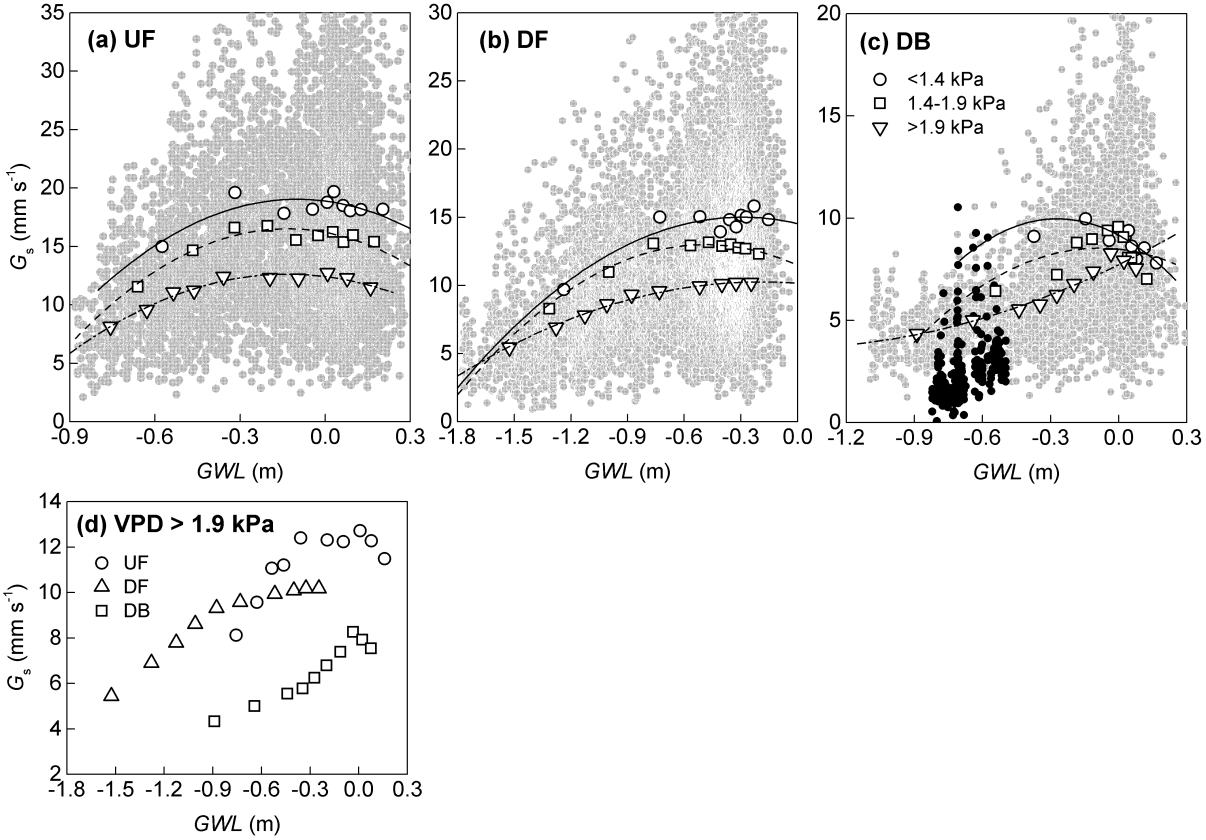
(a) UF
(b) DF
(c) DB
<1.4 kPa
1.4-1.9 kPa
>1.9 kPa
(d) VPD > 1.9 kPa
UF
DF
DB
G_s (mm s^{-1})
GWL (m)

Fig. 5